Detection of Small Hypervascular Hepatocellular Carcinomas in Cirrhotic Patients: Comparison of Superparamagnetic Iron Oxide-Enhanced MR Imaging with Dual-Phase Spiral CT

Jeong-Min Lee, MD[1,2]
In-Hwan Kim, MD[3]
Hyo-Sung Kwak, MD[3]
Ji-Hyun Youk, MD[3]
Young-Min Han, MD[3]
Chong-Soo Kim, MD[3]

[1]Department of Diagnostic Radiology,
Seoul National University Hospital, Seoul,
Korea; [2]Department of Radiation Medicine,
Seoul National University Medical
Research Center, Seoul, Korea; [3]Department of Diagnostic Radiology, Chonbuk
National University Hospital, Chonju,
Korea

Address reprint requests to:
Jeong-Min Lee, MD, Department of
Diagnostic Radiology, Seoul National
University Hospital, 28 Yongon-dong,
Chongno-gu, Seoul 110-744, Korea.
Telephone: (822) 760-3154
Fax: (822) 743-6385
e-mail: leejm@radcom.snu.ac.kr

Objective: To compare the performance of superparamagnetic iron oxide (SPIO)-enhanced magnetic resonance (MR) imaging at 1.5T and dual-phase spiral computed tomography (CT) for the depiction of small hypervascular hepatocellular carcinomas (HCCs).

Materials and Methods: Forty-three patients with 70 small nodular HCCs (5 – 20 mm; mean, 13.7 mm) were examined. Diagnosis was based on the results of surgical biopsy in 22 patients and by the combined assessment of MR imaging, lipiodol CT, alpha feto-protein levels, and angiographic findings in 21. MR imaging consisted of respiratory-triggered turbo spin-echo T2-weighted imaging, T1-weighted fast low-angle shot, and T2*-weighted fast imaging with steady-state precession imaging before and after SPIO enhancement. CT imaging was performed with 5-mm collimation and 1:1.4 pitch, and began 30 and 65 secs after the injection of 150 mL of contrast medium at a rate of 3 mL/sec. Two blinded observers reviewed all images independently on a segment-by-segment basis. Diagnostic accuracy was evaluated using receiver operating characteristics (ROC) analysis.

Results: The mean areas (Az) under the ROC curves were 0.85 for SPIO-enhanced MR imaging and 0.79 for dual-phase spiral CT ($p < .05$). The mean sensitivity of SPIO-enhanced MR imaging was significantly higher than that of CT ($p < .05$), i.e. 70.6% for MR imaging and 58.1% for CT. MR imaging had higher false-positive rates than dual-phase spiral CT, but the difference was not statistically significant (3.7% vs 3.3%) ($p > .05$).

Conclusion: SPIO-enhanced MR imaging is more sensitive than dual-phase spiral CT for the depiction of small hypervascular hepatocellular carcinomas.

Hepatocellular carcinoma (HCC) is one of the most common globally occurring malignant neoplasms. Although hepatic resection is an effective treatment for HCC patients, the resectability, operative mortality, and prognosis for small HCCs differ from those for larger tumors such as those usually found in patients presenting with symptoms (1–5). For large tumors, the operative mortality rate ranges from 6.7% to 36% (3–4), but for small tumors, this rate is 3-12.5% (5). In addition, the five-year survival rate is much better for smaller than for larger tumors. The need for a preoperative imaging modality that can detect small HCCs prior to the appearance of clinical symptoms is thus of great importance in clinical practice.

Contrast-enhanced spiral CT is the most widely used imaging technique for the detection and characterization of focal hepatic lesions. Various studies have shown that the use of dual-phase spiral CT imaging during both the arterial and portal venous

phases of enhancement leads to further improvement in the detection rates of hypervascular tumors such as HCC (6–8). However, the detection of hepatocellular carcinoma and hepatocytic nodules such as dysplastic nodules is difficult because cirrhotic liver parenchyma contains fibrosis, regenerative nodules, fatty infiltration, and parenchymal necrosis (9). Currently, MR imaging is increasingly utilized for the detection of hepatic lesions, and the use of superparamagnetic iron oxide (SPIO), a tissue-specific contrast agent, has the potential to increase the sensitivity and specificity of hepatic MR imaging (10–12). To our knowledge, no study has focused on the comparison of dual-phase contrast-enhanced spiral CT and SPIO-enhanced MR imaging for the detection of small HCCs (less than 2 cm). In the present study, we compare the performance of MR imaging after the administration of SPIO with that of dual-phase contrast-enhanced CT for the detection of small-diameter hypervascular HCCs using receiver operating characteristics (ROC) analysis.

SUBJECTS AND METHODS

Patients

Between October 1998 and January 2002, 120 patients with suspected focal liver tumors underwent dual-phase spiral CT, unenhanced MR imaging, and SPIO-enhanced MR imaging. We excluded 77 of these, as follows: 49 with HCCs larger than 2 cm in diameter; seven in whom hypervascularity of the tumor was not apparent at selective hepatic angiography; seven who underwent radiofrequency thermal ablation; five who underwent surgery more than 4 weeks after CT or MRI; and nine who, after transcatheter arterial chemoembolization (TACE), were not available for follow-up studies of at least 6 months due to a lack of firm evidence of a true-negative segment. The remaining 43 patients, for whom there was acceptable proof of the presence of small hypervascular hepatocellular carcinoma (less than 2 cm in diameter), and who had liver cirrhosis, were included in this study.

In all these patients, liver cirrhosis was determined by clinical examination and blood chemistry tests (aspartate aminotransferase, alanine aminotransferase, alkaline phosphatase, bilirubin, albumin, and globulin). The interval between SPIO-enhanced MR imaging and dual-phase spiral CT was not greater than one month. Direct comparison between MR imaging and CT was made in each imaging section of the liver.

Lesion Confirmation

A total of 43 patients with 70 small HCCs (5–20 mm, mean 13.7 mm) were enrolled in the study. Twelve pa-

tients had two HCCs, one patient had three, three patients had four, and one patient had five, and in each of the remaining 26 patients, one nodule was present. Proof of hypervascular HCC was confirmed using a combination of pathologic and angiographic findings (n=25) or a combination of angiographic and lipiodol CT findings (n=45). Seventeen patients with 20 lesions underwent hepatic resection and intraoperative ultrasonography. In five patients, only one attempt was made to perform percutaneous biopsy of a single lesion per patient, but in three, additional lesions were detected by both lipiodol and angiographic CT. For the other 21 patients with 39 lesions who underwent TACE, the presence of individual malignant lesions was confirmed by means of elevated serum αFP levels, angiographic findings, and lipiodol CT uptake.

Subsegmental TACE was performed by injecting a chemotherapeutic drug emulsion, followed by gelatin sponge particles (Gelfoam; Pharmacia-Upjohn, Mich, U.S.A.), as previously described (13). The emulsion consisted of lipiodol (Guerbet, Aulnay-sous-Bois, France), doxorubicin hydrochloride (Adriamycin; Ildong Pharm Co., Seoul, Korea) and non-ionic contrast material (Ultravist 300; Schering, Berlin, Germany). After performing subsegmental TACE, 2–3 mL of lipiodol was injected into the proper hepatic artery in order to detect hidden HCC at subsequent lipiodol CT, performed using a Somatom Plus-4 scanner (Siemens Medical Systems, Erlangen, Germany) with 5-mm slice thickness two weeks after TACE. The diagnostic criterion for HCC at lipiodol CT was a round, dense deposit of iodized oil after TACE in which this oil was used (14).

Follow-up CT examinations were performed 6–36 months later in all patients who had undergone resective surgery or TACE. Proof of the absence of HCC nodules in hepatic segments was provided by negative findings at intraoperative ultrasonography, or a combination of no nodular lipiodol uptake at lipiodol CT and no evidence of further nodular growth at follow-up CT.

MR Imaging Examinations

All MR imaging was performed on a 1.5-T system (Magnetom Vision; Siemens, Erlangen, Germany) using a phased-array coil for signal reception. Baseline MR images were acquired with a respiratory-triggered T2-weighted turbo spin-echo (TSE) sequence, a breath-hold T2*-weighted fast imaging with steady-state precession (FISP) sequence, and a breath-hold T1-weighted fast low-angle shot (FLASH) sequence.

Respiratory-triggered T2-weighted TSE imaging (TR range/TE, 3300–5500/85) was performed with an echo-train length of 5, a 120×256 matrix, and two signal aver-

ages. Breath-hold T2*-weighted FISP imaging (180/12, 30° flip angle, matrix of 96 × 256, one signal average) was followed by breath-hold T1-weighted FLASH imaging (120/4, 80° flip angle, matrix of 140 × 256, one signal average). All images were obtained in the transaxial plane, using a phased-array multicoil. For all sequences, a 7-mm slice thickness was used, with a 10% intersection gap and a field of view of 35 – 40 cm, depending on the size of the liver.

SPIO-enhanced MR imaging comprised the respiratory-triggered T2-TSE sequence, the breath-hold T2*-weighted FISP sequence, and the breath-hold T1-weighted FLASH sequence, with the same parameters as those used in baseline MR imaging. The SPIO agent (Feridex; Advanced Magnetics, Cambridge, Mass., U.S.A.), was administered at a dose of 15 μmol of iron per kilogram of body weight, was diluted in 100 mL of 5% dextrose solution and injected intravenously through a specific 5 μ filter for 30 mins; imaging commenced approximately 70 (range, 50 – 90) mins after the intravenous infusion of SPIO.

CT Examinations

For dual phase contrast-enhanced spiral CT, a Somatom plus 4 scanner (Siemens Medical Systems, Erlangen, Germany) was used. The scanning parameters were 120 kVp, 240 mA, 5-mm collimation, table speed of 7-mm/sec, and a 5-mm reconstruction interval. After unenhanced spiral liver scanning, the arterial phase was begun 30 secs after the power injection of 150 mL of nonionic contrast material (Iopromide [Ultravist 370]; Schering, Berlin, Germany) at a rate of 3 mL/sec. Portal phase scanning was begun 65 secs after the start of contrast injection.

Imaging Analysis (Receiver Operating Characteristics Analysis, ROC)

Before performing ROC analysis, a gold standard for the lesions to be investigated was defined by two experienced abdominal radiologists, who coordinated ROC analysis and reached their decisions by consensus. They analyzed all the images obtained as well as the operative, laboratory, and histological findings, evaluating a total of 70 separate focal HCC lesions smaller than 2 cm in diameter.

Two other independent observers, both experienced abdominal radiologists, reviewed the contrast-enhanced spiral CT and SPIO-enhanced MR images. They were informed only that the patients with liver cirrhosis were referred for preoperative assessment of suspected liver malignancy. Images were reviewed on a segment-by-segment basis, and to avoid incorrect localization of the lesions, hepatic segmentation according to the Couinaud numbering system was drawn directly. A total of 344 segments (61 of which contained 70 HCC nodules, and 283 segments with-

out proof of the presence of HCC lesions) were reviewed. Five of the 61 segments contained more than two nodules, and to ensure correct localization, each observer recorded the image number and size of each lesion, and added further comments.

Each observer read two sets of images (set 1: unenhanced and SPIO-enhanced turbo spin-echo, T1-weighted FLASH, and T2*-weighted FISP images; set 2: pre- and post-contrast dual-phase spiral CT images), with an interval of at least a week between the two readings. Each recorded the presence and location of one or more lesions, assigning to each a confidence level on a five-point scale: '1' was defined as 'definitely or almost definitely absent'; '2' as 'probably absent'; '3' as 'possibly present'; '4' as 'probably present'; and '5' as 'definitely or almost definitely present'.

For each imaging set, a binomial ROC curve was fitted to each reviewer's confidence rating data using a maximum likelihood estimation (ROCKIT 0.9, Charles E. Metz). The diagnostic accuracy of each imaging modality was determined by calculating the area (A index, Az) under each observer-specific binomial ROC curve plotted in the designed square. The composite ROC curves used to represent the combined performance of the two observers were calculated for each set of images using Rockit 0.9 software to rate their pooled data. The differences between imaging modalities in terms of the mean areas under the ROC curves were statistically analyzed using the two-tailed Student t test for paired data. To determine relative sensitivity for HCC, the number of segments assigned level 3 or more from among the 70 HCC nodules was noted. The relative sensitivities and specificities for HCC obtained from the two radiologists' and pooled data were calculated for each modality, and to ascertain the differences between the imaging modalities and between observers, multiple comparisons involving Student's t test were made. A two-tailed p value of less than 0.05 was considered significant.

Agreement between blinded observers is reported below in terms of kappa values, those greater than 0 indicating positive correlation. Values of up to 0.4 indicated positive but poor correlation; those of 0.41 – 0.75 indicated good correlation.

RESULTS

For all 70 lesions, the calculated areas under the ROC curves and the mean area for the two observers for each imaging modality are shown in Table 1. For each modality, ROC curves drawn on the basis of the data pooled by the two observers are shown in Figure 1. In terms of lesion detection, both agreed that performance using the set of

SPIO-enhanced MR images was significantly superior to that obtained at dual-phase spiral CT imaging ($p < .05$). The mean area under both observers' ROC curves was 0.85 for pre- and post-SPIO-enhanced MR imaging and 0.79 for pre- and post-contrast dual-phase spiral CT imaging; this difference was statistically significant ($p < .05$).

Sensitivities and specificities were calculated for each observer and for each modality, and mean values were also determined (Table 2). The combination of SPIO-enhanced MR images was 12.5% more sensitive than that of dual-phase spiral CT images (MR, 70.6%; CT, 58.1%), a statistically significant difference ($p < .05$). In 18 cases, tumor nodules were detected at MR imaging, but not at CT. In 12 cases, nodules were smaller than 1cm (Fig. 2). In two cases, additional lesions were detected only at CT; in one of these, because the high signal intensity of the gallbladder (GB) interfered with the signal intensity of the true nodule, found at T2-weighted imaging to also be high, the observers missed a 5-mm subcapsular nodule abutting the GB. In the other case, a small nodule was not detected because of the presence of severely injured liver parenchyma of heterogeneous texture. In addition, 11/70 lesions (15.7%) in ten patients were not detected by any modality.

Table 1. Individual and Mean Areas Under the Curve for Pre- and Post-SPIO-Enhanced MR and Dual-Phase Spiral CT (All Lesions)

Imaging Modality	Az Index		
	Observer 1	Observer 2	Mean
CT imaging	0.80±0.03	0.78±0.04	0.79±0.02
MR imaging	0.86±0.03*	0.85±0.03*	0.85±0.02

Note.— Values are expressed as mean ±SD.
*For the comparison of MR imaging with CT, $p < .05$

Table 2. Sensitivity and Specificity of Pre- and Post-SPIO-Enhanced MR and Dual-Phase Spiral CT (All Lesions)

Imaging Modality	Az Index		
	Observer 1	Observer 2	Mean
CT			
Sensitivity	58.8	57.4	58.1
Specificity	96.5	96.9	96.7
MR			
Sensitivity	72.1*	69.1*	70.6*
Specificity	96.2	95.5	95.8

Note.— Numbers are percentages.
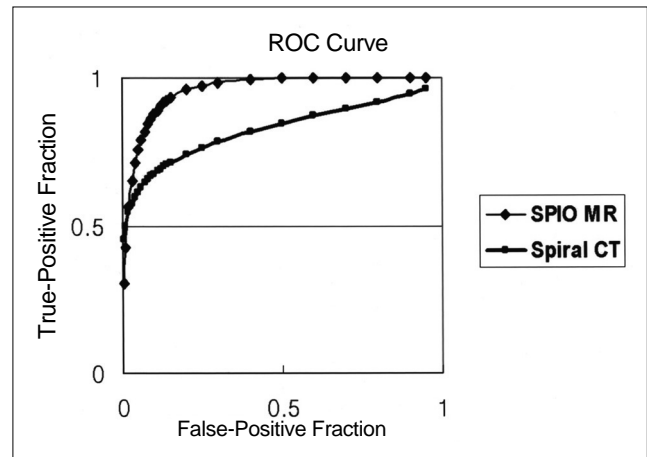*For the comparison of MR imaging with CT, $p < .05$

Fig. 1. ROC curves describe observer confidence in the detection of hepatocellular carcinomas depicted at pre- and post-SPIO-enhanced MR imaging involving T1-weighted FLASH, T2-weighted TSE, and T2*-weighted FISP sequences (diamonds), and another set obtained at contrast-enhanced dual-phase spiral CT (squares). Note that observers showed more confidence in interpreting MR images than dual-phase spiral CT images ($p < .05$).

Fig. 2. In this 63-year-old man, a 0.8-cm hepatocellular carcinoma was found in segment I.
A. Neither the arterial-phase CT image (left) nor the portal venous-phase CT image (right) revealed the presence of a lesion.
B. SPIO-enhanced respiratory-triggered T2-weighted turbo spin-echo image (left) and breath-hold T2*-weighted fast image obtained with steady state precession (right) depict the tumor as an area of high signal intensity (arrows). Its presence was surgically confirmed.

Of these false-negative lesions, three were confirmed by percutaneous biopsy, two by surgical resection and biopsy, and the remaining six by lipiodol CT. Except for one with a diameter of 2 cm, these missed lesions ranged in size from 0.5 to 1.0 cm. The 2.0-cm nodule was located in the subcapsular dome of segment VIII and was therefore misinterpreted at both CT and MR imaging as a partial volume artifact of the cardiac structure.

In terms of specificity, CT was superior to MR imaging (96.7% versus 96.3%) though this difference was not statistically significant ($p > .05$). At CT, the observers detected 13 false-positive lesions, all of which were attributed to the perfusion artifact (Fig. 3), and at MR imaging, a total of 15 false-positive lesions were detected; most were attributed to misdiagnosis of the intrahepatic vessels as tumor nodules (Fig. 4).

For CT and MR imaging, kappa values for the two observers were 0.698 and 0.723, respectively, indicating good inter-observer agreement.

DISCUSSION

Recent studies have shown that for the detection of focal hepatic lesions, SPIO-enhanced MR imaging is considerably more sensitive than conventional contrast-enhanced CT and unenhanced MR imaging, and is at least as accurate as CT during arterial portography (CTAP) (15–21). In addition, previous studies have indicated that the results of SPIO-enhanced MR imaging were comparable to those of dual-phase contrast-enhanced CT (20). However, unlike metastatic tumors, most HCCs occur in chronically injured liver tissue that shows less response to iron oxide particles than does normal liver tissue (22).

In this study, we compared the accuracy of SPIO-enhanced MR imaging and dual-phase spiral CT for the detection of small HCCs in patients with liver cirrhosis, showing that the former was more accurate than the latter ($p < .05$). ROC analysis indicated that both observers performed better with SPIO-enhanced MR imaging than with
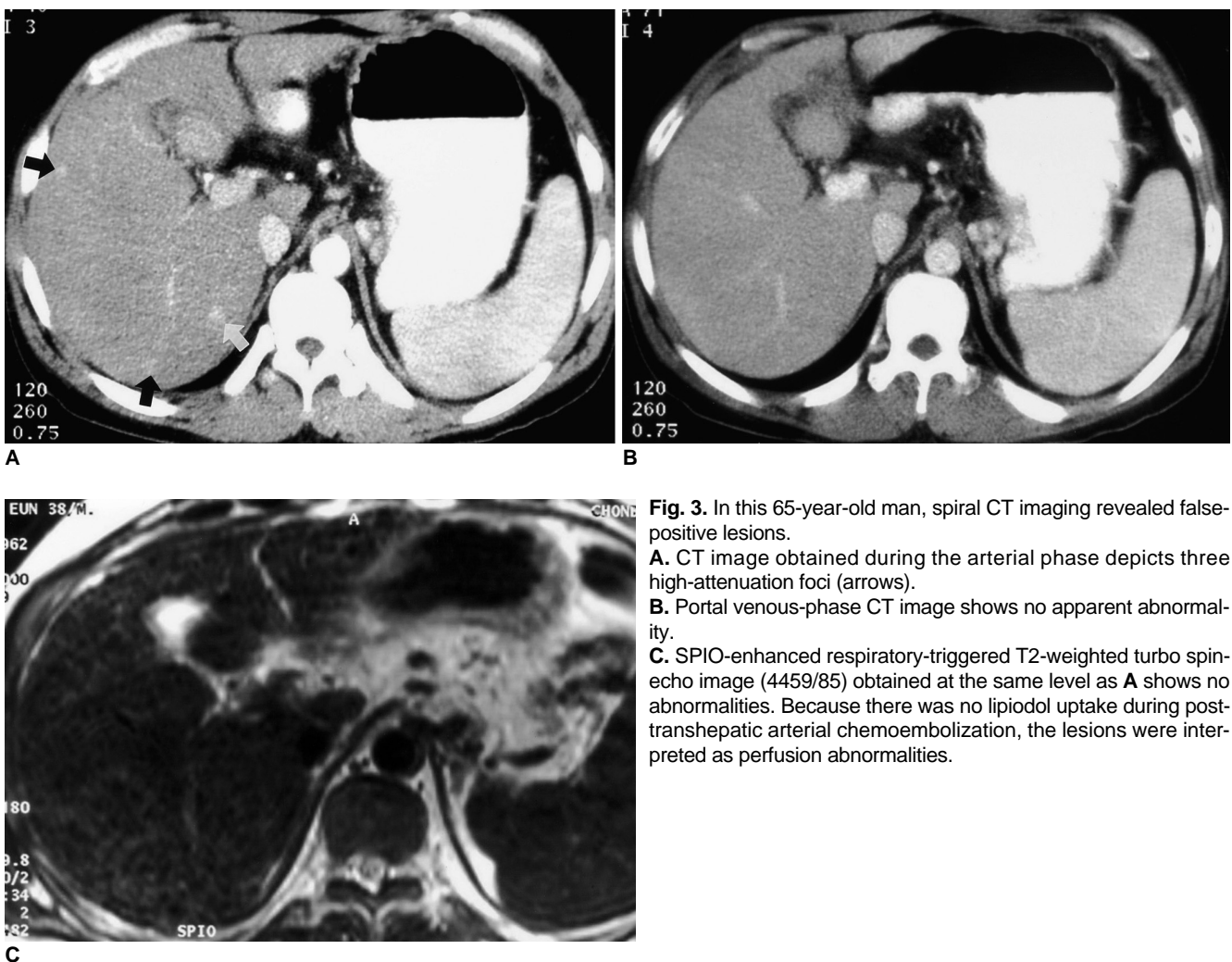
A

B

C

Fig. 3. In this 65-year-old man, spiral CT imaging revealed false-positive lesions.
A. CT image obtained during the arterial phase depicts three high-attenuation foci (arrows).
B. Portal venous-phase CT image shows no apparent abnormality.
C. SPIO-enhanced respiratory-triggered T2-weighted turbo spin-echo image (4459/85) obtained at the same level as **A** shows no abnormalities. Because there was no lipiodol uptake during post-transhepatic arterial chemoembolization, the lesions were interpreted as perfusion abnormalities.
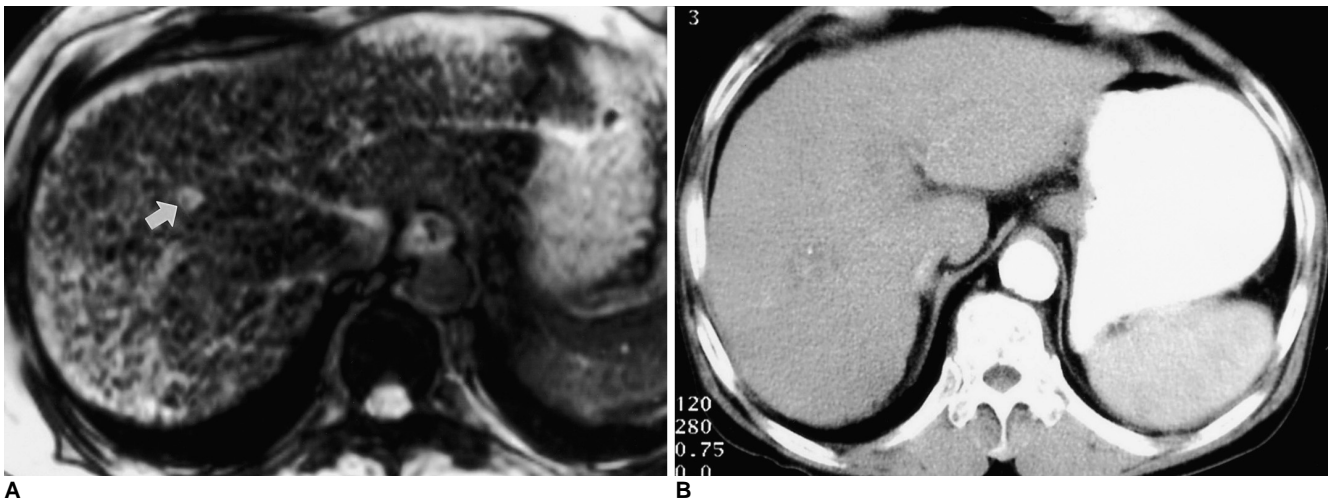
Fig. 4. In this 45-year-old man, a false-positive lesion was seen at SPIO-enhanced MR imaging.
A. SPIO-enhanced breath-hold T2∗-weighted fast MR image obtained with steady-state precession (180/12, 30° flip angle) reveals a high-signal-intensity focal area (arrow).
B. Arterial-phase CT image obtained at the same level as **A** depicts no abnormalities. The presence of this false-positive lesion at MRI is attributed to misinterpretation of the vessel as a tumor nodule.

spiral CT (Table 1).

In this study, the sensitivity of SPIO-enhanced MR imaging was relatively low compared to the findings of previous reports (15−17, 19) (Table 2). This difference arose, we believe, because the tumors were small and because liver enhancement was poor due to the decreased activity of Kupffer's cells. In addition, more prominent visualization of the reticular fibrosis occurring in cirrhotic liver and the difficulty of differentiating vascular structures from small tumor nodules may be important causes of the lower sensitivity of MR imaging, compared with previous findings. Because of these problems with SPIO-enhanced MR imaging, the sensitivity of HCCs smaller than 2 cm showed no further increase. Other reports, however, have noted a similar sensitivity for lesions less than 2 cm in diameter (20); Choi et al. (17) mentioned that in their series, the lesions missed at MR imaging were also smaller than 2 cm.

The specificity of dual-phase spiral CT was similar to that of SPIO-enhanced MR imaging (Table 2). The former showed false-positive findings involving lesions arising from a small arteriovenous shunt. Because an arterioportal shunt is detected as a hyperenhancing focus during the arterial dominant phase of dynamic studies and as a portal venous perfusion defect similar to hepatocellular carcinoma at CTAP, a non-tumorous arterioportal shunt in cirrhotic liver can sometimes mimic HCC at dynamic CT (23, 24). The administration of SPIO led to decreased hepatic parenchymal signal intensity, and the enhanced vascular structure was thus seen as a focal nodular form and was misinterpreted as a nodule. In addition, clearer visualiza-

tion of the parenchymal fibrosis occurring in cirrhotic liver made it difficult to differentiate fibrosis from a tumor. According to previous reports regarding the value of SPIO-enhanced MR imaging for the detection of focal liver lesions, the high signal intensity of vascular structures (vessels mimicking nodules) was the most frequent cause of false-positive interpretations (17, 19).

Our choice of MR sequence before and after SPIO enhancement requires further explanation. To achieve the best results that SPIO can provide, the selection of suitable pulses is essential. To maximize the detection of small HCCs, we obtained a set of pre- and post-SPIO-enhanced images using a T2*-weighted FISP sequence, T1-weighted FLASH imaging, and a respiratory-triggered T2-weighted TSE sequence. It is clear from various comparative studies that gradient-recalled echo pulse sequences can be used to enforce local field inhomogeneities to T2* relaxation and to achieve brilliant lesion-to-liver contrast (16, 25−28). In addition, we used respiratory-triggered TSE imaging rather than conventional spin-echo or breath-hold TSE imaging. Because TSE sequences use more refocusing pulses and are less prone to the magnetic susceptibility effect, conventional spin-echo imaging is more sensitive than TSE (26, 27). In addition, at many institutions, breath-hold TSE imaging has replaced conventional spin-echo or respiratory-triggered TSE imaging for routine T2-weighted imaging of the liver. However, we used a respiratory-triggered TSE sequence for two reasons: because the conventional spin-echo sequence, which requires prolonged acquisition time, increases the imaging artifact in cirrhotic patients, and because as-

cites formation related to poor liver function in patients with liver cirrhosis makes long breath-holding very difficult. Because a benign cyst shows low signal intensity at SPIO-enhanced MR imaging, despite the high signal intensity of other malignant lesions, and an hemangioma shows increased signal intensity at SPIO-enhanced T1-weighted imaging (29, 30), we used the T1-weighted gradient-echo sequence to differentiate HCC from hemangioma and cyst.

This study suffers certain limitations. First, there was insufficient histopathologic confirmation of the presence of liver lesions. Although most lesions not subject to biopsy probably represent additional sites of HCC or true-positive lesions, some false-positive lesions might have been included in our study. Second, because only 17 patients underwent surgery and intraoperative ultrasonography, it was not absolutely certain that in segments apparently without HCC nodules, these were in fact absent (true negative). However, we used relatively strict criteria for the standard of reference regarding true-negative segments, i.e. negative CT findings after the arterial infusion of iodized oil were combined with follow-up CT at least six months later. Third, we performed arterial and portal phase imaging after contrast injection. Because some small HCCs may show iso-attenuation to surrounding liver parenchyma at portal phase imaging, the inclusion of equilibrium phase imaging may increase the likelihood of observing the contrast washout effect of HCCs and therefore improve the detection rate for small HCCs (31, 32). Last, the spiral CT technology used in this study was not state of the art. Multidetector spiral CT now permits the use of thinner slice thicknesses and better time resolution than is possible with single-detector mode (33), and we believe that its use may improve the accuracy of CT examinations for the evaluation of focal liver tumors.

In conclusion, MR imaging performed before and after the administration of SPIO contrast material and involving combined T2- and T2*- weighted sequences and an additional T1-weighted sequence is more sensitive and accurate than dual-phase spiral CT imaging for the detection of small HCCs. To detect these, a set of SPIO-enhanced MR imaging sequences can thus be used in place of dual-phase spiral CT imaging as a preoperative diagnostic strategy in patients with cirrhosis or other chronic disease of the liver.

References

1. Adson MA, Weiland LH. Resection of primary solid hepatic tumors. *Am J Surg* 1981;141:18-21
2. Lim RC, Bongard FS. Hepatocellular carcinoma. *Arch Surg* 1984;119:637-642
3. Fortner JG, Kim DK, Maclean BJ, et al. Major hepatic resection for neoplasia: personal experience in 108 patients. *Ann Surg* 1978;188:363-369
4. Iwatsuki S, Shaw BW, Starzl TE. Experience with 150 liver resections. *Ann Surg* 1983;197:247-253
5. Kanematsu T, Takenaka L, Matsumata T, Furnita T, Sugimachi K, Inokuchi K. Limited hepatic resection effective for selected cirrhotic patients with primary liver cancer. *Ann Surg* 1984; 199:51-56
6. Lee KH, Choi BI, Han JK, Jang HJ, Kim TK, Han MC. Nodular hepatocellular carcinoma: variation of tumor conspicuity on single-level dynamic scan and optimization of fixed delay times for two-phase helical CT. *J Comput Assist Tomogr* 2000;24:212-218
7. Kim T, Murakami T, Takahash S, et al. Optimal phases of dynamic CT for detecting hepatocellular carcinoma: evaluation of unenhanced and triple-phase images. *Abdom Imaging* 1999;24: 473-480
8. Yamashita Y, Mitsuzaki K, Yi T, et al. Small hepatocellular carcinoma in patients with chronic liver damage: prospective comparison of detection with dynamic MR imaging and helical CT of whole liver. *Radiology* 1996;200:79-84
9. Miller WJ, Baron RL, Dodd GD III, Federle MP. Malignancies in patients with cirrhosis: CT sensitivity and specificity in 200 consecutive transplant patients. *Radiology* 1994;193:645-650
10. Winter TC III, Freeny PC, Nghiem HV, et al. MR imaging with IV superparamagnetic iron oxide: efficacy in the detection of focal hepatic lesions. *AJR Am J Roentgenol* 1993;161:1191-1198
11. Ros PR, Freeny PC, Harms SE, et al. Hepatic MR imaging with ferumoxides: a multicenter clinical trial of its safety and efficacy in the detection of focal hepatic lesions. *Radiology* 1995; 196:481-488
12. Soyer P. Will ferumoxides-enhanced MR imaging replace CT during arterial portography in the detection of hepatic metastases? Prologue to a promising future. *Radiology* 1996;200: 610-611
13. Matsui O, Kadoya M, Yoshikawa J, et al. Small hepatocellular carcinoma: treatment with subsegmental transcatheter arterial embolization. *Radiology* 1993;188:79-83
14. Kubota K, Hisa N, Nashikawa T, et al. Evaluation of hepatocellular carcinoma after treatment with transcatheter arterial chemoembolization: comparison of Lipiodol CT, power Doppler sonography, and dynamic MRI. *Abdom Imaging* 2001;26:184-190
15. Yamamoto H, Yamashita Y, Yoshimatsu S, et al. Hepatocecullular carcinoma in cirrhotic livers: detection with unenhanced and iron oxide-enhanced MR imaging. *Radiology* 1995;195: 106-112
16. Tang Y, Yamashita Y, Arakawa A, et al. Detection of hepatocellular carcinoma arising in cirrhotic livers: comparison of Gadolinium-and Ferumoxides-enhanced MR imaging. *AJR Am J Roentgenol* 1999;172:1547-1554
17. Choi D, Kim SH, and Lim JH, et al. Preoperative detection of hepatocellular carcinoma: ferumoxides-enhanced MR imaging versus combined helical CT during arterial portography and CT hepatic arteriography. *AJR Am J Roentgenol* 2001;176:475-482
18. Hagspiel KD, Neidl KFW, Eichenberger AC, Weder W, Marincek B. Detection of liver metastases: comparison of super-

paramagnetic iron oxide-enhanced MR imaging at 1.5-T with dynamic CT, intraoperative US and percutaneous US. *Radiology* 1995; 196:471-478

19. Ward J, Naik KS, Guthrie JA, Wilson D, Robison PJ. Hepatic lesion detection: comparison of MR imaging after the administration of superparamagnetic iron oxide with dual-phase CT by using alternative free-response receiver operating characteristic analysis. *Radiology* 1999;210:459-466

20. Bluemke DA, Paulson EK, Choti MA, DeSena S, Clavien PA. Detection of hepatic lesions in candidates for surgery: comparison of ferumoxides-enhanced MR imaging and dual-phase helical CT. *AJR Am J Roentgenol* 2000;175:1653-1658

21. Seneterre E, Taourel P, Bouvier Y, et al. Detection of hepatic metastases: ferumoxides-enhanced MR imaging versus unenhanced MR imaging and CT during arterial portography. *Radiology* 1996;200:785-792

22. Elizondo G, Weissleder T, Stark DD, et al. Hepatic cirrhosis and hepatitis: MR imaging enhanced with superparamagnetic iron oxide. *Radiology* 1990;174:797-801

23. Kim TK, Choi BI, Han JK, Chung JW, Park JH, Hand MC. Nontumorous arterioportal shunt mimicking hypervascular tumor in cirrhotic liver: two-phase spiral CT findings. *Radiology* 1998;208:597-603

24. Choi BI, Lee KH, Han JK, Lee JM. Hepatic arterioportal shunt: dynamic CT and MR features. *Korean J Radiol* 2002;3:1-15

25. Josephson L, Lewis J, Jacob P, Hahn PF, Stark DW. The effects of iron oxides on proton relaxivity. *Magn Reson Imaging* 1988;6:647-653

26. Ward J, Chen F, Guthrie JA, et al. Hepatic lesion detection after superparamagnetic iron oxide enhancement: comparison of five

T2-weighted sequences at 1.0T by using alternative free-response receiver operating characteristic analysis. *Radiology* 2000;214:159-166

27. Schwartz LH, Seltzer SE, Tempany CM, et al. Superparamagnetic iron oxide hepatic MR imaging: efficacy and safety using conventional and fast spin-echo pulse sequences. *J Magn Reson Imaging* 1995;5:566-570

28. Kim SH, Choi DI, Lim JH, et al. Optimal pulse sequence for ferumoxides-enhanced MR imaging used in the detection of hepatocellular carcinoma: comparative study using seven pulse sequences. *Korean J Radiol* 2002;3:87-97

29. Oudkerk M, van den Heuvel AG, Wielopolski PA, Shmits PIM, Borel Rinkes IHM, Wiggers T. Hepatic lesions: detection with ferumoxides-enhanced T1-weighted MR imaging. *Radiology* 1997;203:449-456

30. Grangier C, Tourniaire J, Mentha G, et al. Enhancement of liver hemangioma on T1-weighted MR SE images by superparamagnetic iron oxide particles. *J Comput Assist Tomogr* 1994;18:888-896

31. Jang HJ, Lim JH, Lee SJ, et al. Hepatocellular carcinoma: are combined CT duing arterial portography and CT hepatic arteriography in addition to triple-phase helical CT all necessary for preoperative evaluation? *Radiology* 2000;215:373-380

32. Lim JH, Choi DI, Kim SH, et al. Detection of hepatocellular carcinoma: value of adding delayed-phase imaging to dual-phase helical CT. *AJR Am J Roentgenol* 2002;179:67-73

33. Murakami T, Kim T, Takamura M, et al. Hypervascular hepatocellular carcinoma: detection with double arterial-phase multidetector row helical CT. *Radiology* 2001;218:763-767